JACS
JOURNAL OF THE AMERICAN CHEMICAL SOCIETY
pubs.acs.org/JACS
Article

# Dual-Channel Fluorescent Probe for the Simultaneous Monitoring of Peroxynitrite and Adenosine-5′-triphosphate in Cellular Applications

Luling Wu,[‡] Jihong Liu,[‡] Xue Tian,[‡] Robin R. Groleau, Beidou Feng, Yonggang Yang, Adam C. Sedgwick, Hai-Hao Han,* Yang Wang, Han-Min Wang, Fang Huang, Steven D. Bull, Hua Zhang,* Chusen Huang,* Yi Zang, Jia Li, Xiao-Peng He, Ping Li,* Bo Tang, Tony D. James,* and Jonathan L. Sessler*

Cite This: *J. Am. Chem. Soc.* 2022, 144, 174−183



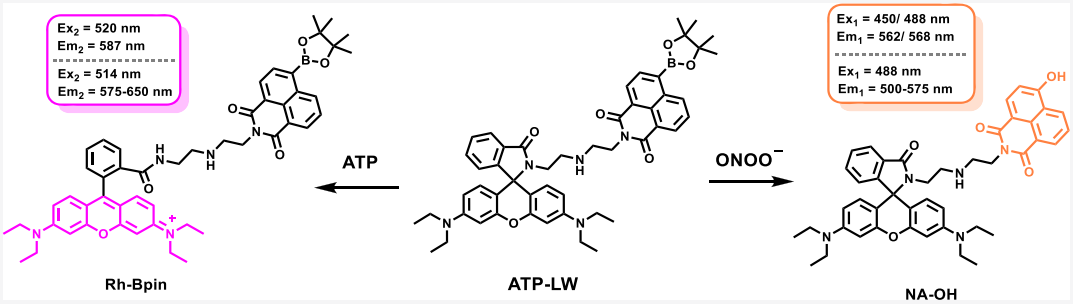


**ABSTRACT:** Changes in adenosine triphosphate (ATP) and peroxynitrite ($ONOO^-$) concentrations have been correlated in a number of diseases including ischemia-reperfusion injury and drug-induced liver injury. Herein, we report the development of a fluorescent probe ATP-LW, which enables the simultaneous detection of $ONOO^-$ and ATP. $ONOO^-$ selectively oxidizes the boronate pinacol ester of ATP-LW to afford the fluorescent 4-hydroxy-1,8-naphthalimide product NA-OH ($\lambda_{ex}$ = 450 nm, $\lambda_{em}$ = 562 nm or $\lambda_{ex}$ = 488 nm, $\lambda_{em}$ = 568 nm). In contrast, the binding of ATP to ATP-LW induces the spirolactam ring opening of rhodamine to afford a highly emissive product ($\lambda_{ex}$ = 520 nm, $\lambda_{em}$ = 587 nm). Due to the differences in emission between the $ONOO^-$ and ATP products, ATP-LW allows $ONOO^-$ levels to be monitored in the green channel ($\lambda_{ex}$ = 488 nm, $\lambda_{em}$ = 500−575 nm) and ATP concentrations in the red channel ($\lambda_{ex}$ = 514 nm, $\lambda_{em}$ = 575−650 nm). The use of ATP-LW as a combined $ONOO^-$ and ATP probe was demonstrated using hepatocytes (HL-7702 cells) in cellular imaging experiments. Treatment of HL-7702 cells with oligomycin A (an inhibitor of ATP synthase) resulted in a reduction of signal intensity in the red channel and an increase in that of the green channel as expected for a reduction in ATP concentrations. Similar fluorescence changes were seen in the presence of SIN-1 (an exogenous $ONOO^-$ donor).

## INTRODUCTION

Adenosine-5′-triphosphate (ATP) has been referred to as the "molecular currency".[1,2] ATP concentrations range between 1 and 10 mM, with a 1000:1 ratio between ATP and adenosine diphosphate (ADP) typically prevailing.[3] ATP aids the regulation of important cellular functions, including cellular movement,[4] neurotransmission,[5] and ion channel function.[6] Disruption to ATP homeostasis is linked to a number of diseases, including ischemia, Parkinson's disease, and hypoglycemia.[7] The cause of this disruption is often ascribed to oxidative stress, which involves the production of highly reactive oxygen species (ROS) and reactive nitrogen species (RNS).[8,9] In particular, peroxynitrite ($ONOO^-$)[10] is an RNS that is known to inhibit ATP production by oxidatively deactivating mitochondrial ATP synthase.[11] Correlations between ATP and $ONOO^-$ concentrations have been observed in a number of pathological events.[12−14] Therefore, the development of a chemical tool that allows the real-time monitoring of these species simultaneously *in vitro* and *in vivo* would be highly desirable.

Fluorescence imaging has emerged as an attractive technology for the real-time and noninvasive detection of biomarkers in cellular and animal-based applications. Pre-

**Received:** July 30, 2021
**Published:** December 21, 2021





https://doi.org/10.1021/jacs.1c07954
*J. Am. Chem. Soc.* 2022, 144, 174−183

**Scheme 1. Chemical Structure of ATP-LW and Its Fluorescence "Turn On" Mechanism in the Presence of $ONOO^-$, ATP, and $ONOO^-$/ATP[a])**

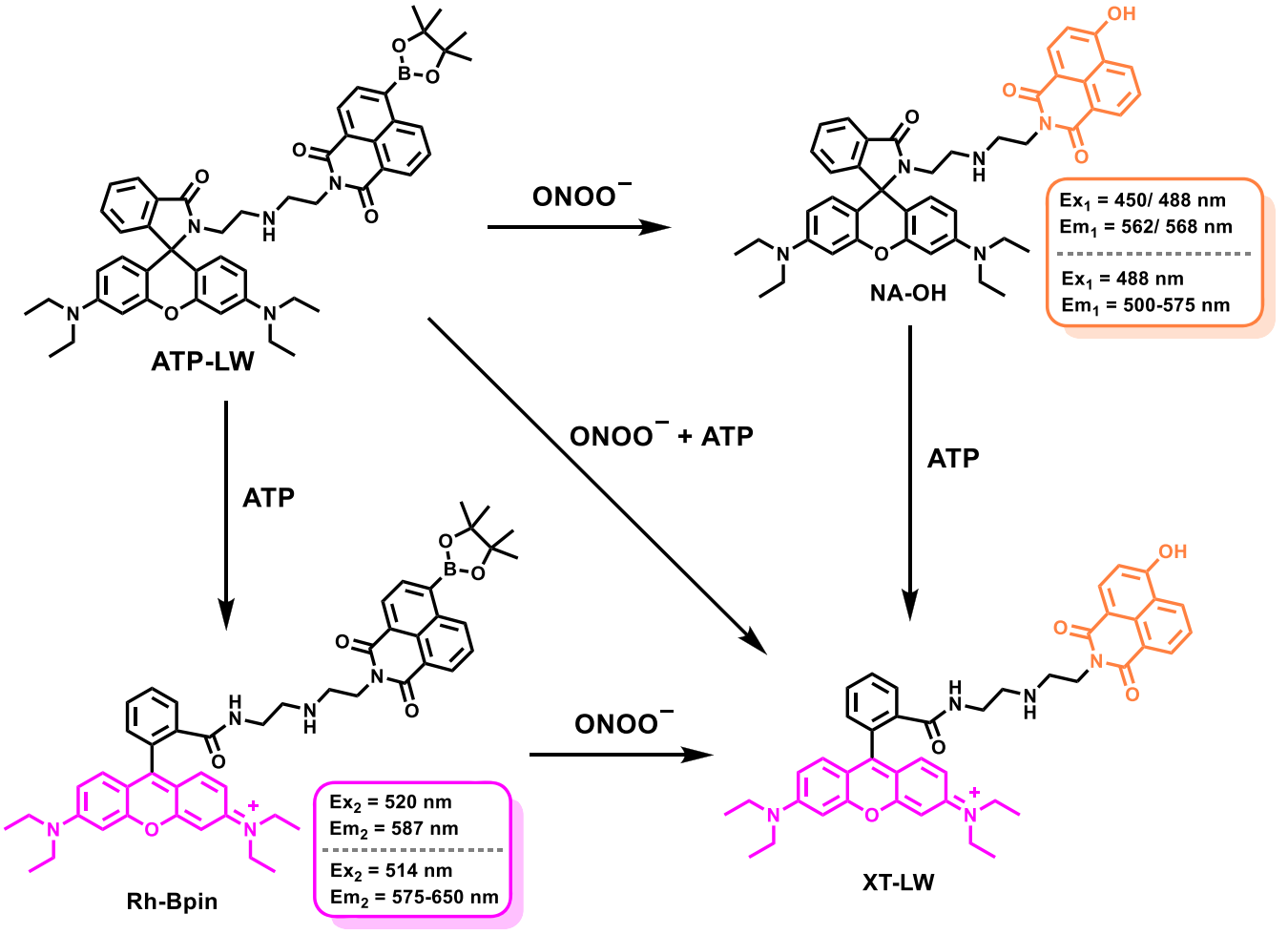


[a]The addition of $ONOO^-$ leads to formation of compound NA-OH, with a maximum emission at 562 nm when excited at 450 nm and a maximum at 568 nm when excited at 488 nm in PBS buffer solution (10 mM, v/v, $EtOH/H_2O$ = 1/99, pH = 7.40). The presence of ATP affords the product Rh-Bpin, with a maximum emission at 587 nm when excited at 520 nm in PBS buffer solution (10 mM, v/v, $EtOH/H_2O$ = 1/99, pH = 7.40).

viously, several single-analyte fluorescent probes have been reported for the selective imaging of $ONOO^-$.[15−17] Moreover, fluorescent probes for the selective detection and visualization of ATP have been developed.[18] However, to our knowledge no fluorescent probes capable of the simultaneous and independent imaging of $ONOO^-$ and ATP have been reported. If available, such systems would allow the presumed close relationship between these two critical species to be monitored in real time. Herein, we report the construction of ATP-LW, a single fluorescent probe that enables the simultaneous detection of $ONOO^-$ and ATP. Initial solution data established excellent water solubility, sensitivity, and high selectivity for $ONOO^-$ and ATP using their respective detection emission profiles. As a preliminary proof-of-concept study for cellular applications, changes in ATP and $ONOO^-$ associated with acetaminophen (APAP) were evaluated. This model was chosen due to the importance of preclinical tools for drug development in the screening of drug-induced liver injury (DILI) associated with drugs like APAP.[19−21] Furthermore, this model was selected because APAP can result in a depletion of ATP and an increase in the levels of $ONOO^-$ (Scheme S1).[22,23] We believe ATP-LW could prove popular as a fluorescent tool in fundamental and clinical research. For example, the Sessler group has been developing type-II immunogenic cell death (ICD) inducers, where the ICD agent results in ROS-mediated ER stress and subsequent ATP release. We anticipate that ATP-LW will facilitate the rapid identification of type-II ICD inducers.[24] It is important to note that we first disclosed our probe ATP-LW as a ChemRxiv preprint;[25] however, we felt that the associated journal contribution (i.e., this article) would be substantially improved with the addition of biological experiments. Unfortunately, the Covid-19 pandemic severely hindered our research progress, and in the time between the ChemRxiv preprint and the present submission, the group of Tian et al. reported a somewhat similar structure for the simultaneous detection of ATP and $H_2O_2$.[26] Pointedly, Merck recognized the potential of ATP-LW and has made it commercially available.[27] However, details regarding the scope, utility, and even mode of use have yet to appear in a peer-reviewed forum. This report is designed to address this deficiency and to highlight the utility of what is now a commercially available fluorescent $ONOO^-$ and ATP probe, ATP-LW.

At this point it is worth discussing the selectivity of boronate ester-based probes toward $ONOO^-$ and $H_2O_2$. Since the seminal report by Sikora et al., numerous research groups,


https://doi.org/10.1021/jacs.1c07954
J. Am. Chem. Soc. 2022, 144, 174−183

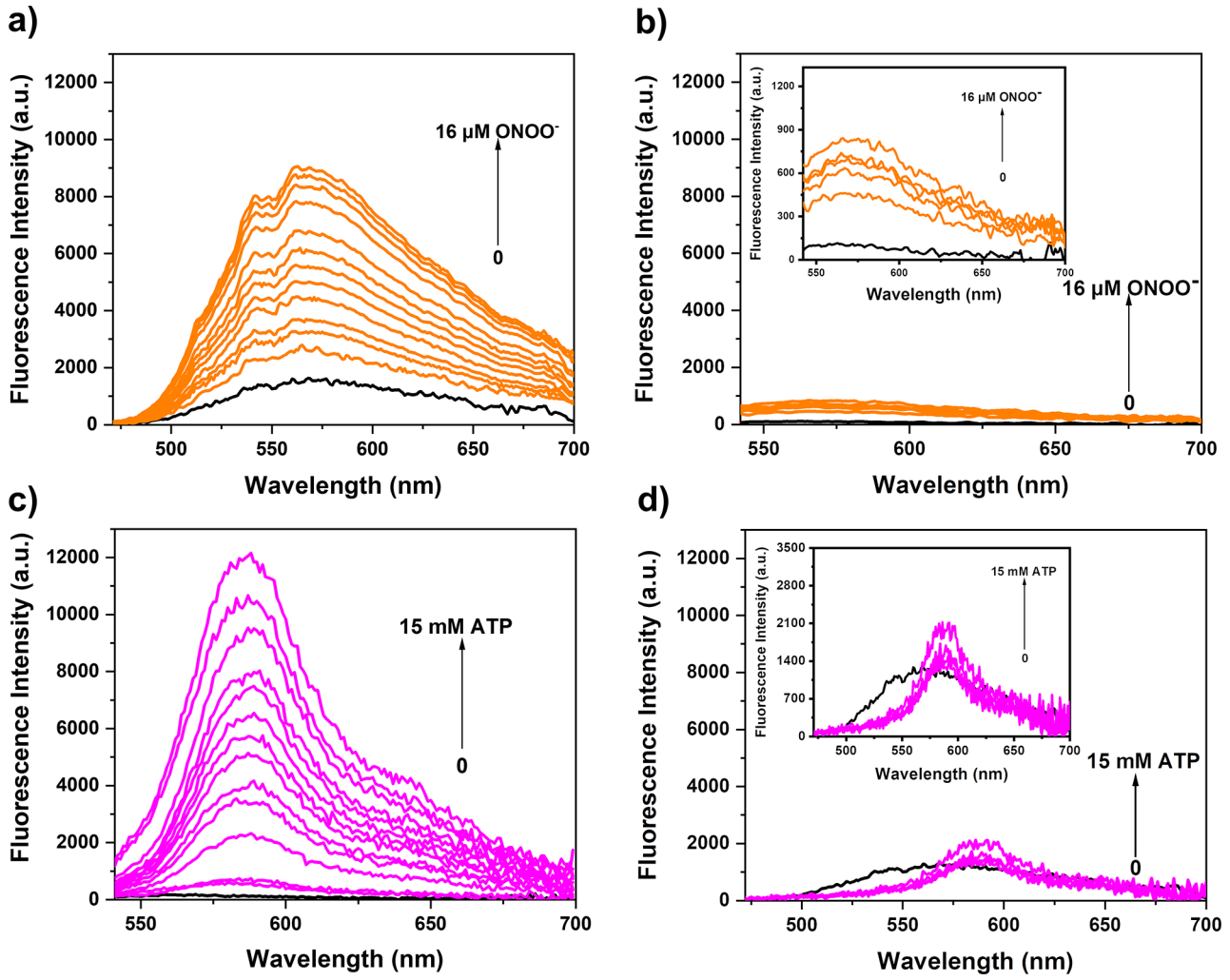


**Figure 1.** Changes in the fluorescence emission intensity of ATP-LW (15 $\mu$M) seen upon the addition of $ONOO^-$ (from 0 to 16 $\mu$M) in modified PBS buffer (10 mM, v/v, $EtOH/H_2O$ = 1/99, pH = 7.40) after 1 min. (a) Sample excited at 450 (bandwidth 8) nm; (b) sample excited at 520 (bandwidth 8) nm. Inset: Enlarged views of the spectra in (b). Changes in the fluorescence emission intensity of ATP-LW (15 $\mu$M) seen upon the addition of ATP (from 0 to 15 mM) in modified PBS buffer solution (10 mM, v/v, $EtOH/H_2O$ = 1/99, pH = 7.40) after 100 min. (c) Sample excited at 520 (bandwidth 8) nm; (d) sample excited at 450 (bandwidth 8) nm. Inset: Enlarged views of the spectra in (d).

including our own, have determined that boronate ester-based fluorescent probes have a preferential reactivity toward $ONOO^-$.[28−30] As such, it is now universally accepted that $ONOO^-$ reacts several orders of magnitude faster than hydrogen peroxide (microseconds vs hours).[31] In addition an observed lack of response toward $ONOO^-$ may indicate degradation of the fluorescent reporter by the highly reactive $ONOO^-$.[20]

In recent years, multianalyte fluorescent probes have garnered attention owing to their enhanced precision for the study in question.[32,33] These systems overcome the problems of using several independent fluorescent probes when seeking to understand the relationship between more than one biological species.[31] Efforts from our group and others have led to the development of multianalyte fluorescent probes.[31] For example, we reported AND-logic gate-like dual-analyte fluorescence scaffolds that permit the detection of $ONOO^-$ and a second analyte.[34−38] However, we believe that systems able to detect more than one analyte independently using different emission channels will prove particularly advantageous;[20] this is because, in principle, dual-channel emission should enable the concurrent evaluation of each individual species, whereas AND-logic systems only provide information on the synergy of the two species.

In this work, we have used a rhodamine lactam/1,8-naphthalimide hybrid structure as a scaffold to create the dual-analyte fluorescent probe ATP-LW (Scheme 1).[39] ATP-LW was synthesized over three steps (Scheme S2). The first step of the synthesis involves a Miyaura borylation reaction, which forms intermediate NA-Bpin. Diethylenetriamine was then added to a solution of rhodamine B in methanol. This reaction afforded intermediate Rh-AM as a light orange solid. Condensation between NA-Bpin and Rh-AM in ethanol then afforded ATP-LW. The chemical structure of ATP-LW was fully characterized using $^1H$ NMR and $^{13}C$ NMR spectroscopy, as well as high-resolution mass spectrometry.

## RESULTS AND DISCUSSION

In initial studies, the changes in the UV−vis absorption spectral features of ATP-LW in the presence of $ONOO^-$ and ATP were investigated in aqueous media (PBS buffer, 10 mM, v/v, $EtOH/H_2O$ = 1/99, pH = 7.40). The addition of $ONOO^-$ produced a new absorption peak at 445 nm, which is


https://doi.org/10.1021/jacs.1c07954
J. Am. Chem. Soc. 2022, 144, 174−183

consistent with the known intramolecular charge transfer (ICT) process seen in 4-hydroxy-1,8-naphthalimide products (Figure S1).[40] Similarly, the addition of ATP to ATP-LW resulted in an increase in the absorption intensity at 553 nm. This was taken as evidence for the ATP-induced opening of the spirolactam ring on the rhodamine fluorophore (Figure S2).[18] ATP-LW was initially nonfluorescent, presumably as the result of quenching by the boronic ester on the 1,8-naphthalimide unit, and the ring-closed form of rhodamine being inherently nonfluorescent. Upon the addition of $ONOO^-$ (0−16 $\mu$M), an increase in the fluorescence intensity at 562 nm/568 nm was observed upon excitation at 450/488 nm (Figure 1a, Figures S7−S10). A minimal fluorescence increase was observed for light excitation at 520 nm upon the addition of $ONOO^-$ (0−16 $\mu$M) (Figure 1b). The formation of a 4-hydroxy-1,8-naphthalimide product upon treatment of ATP-LW with $ONOO^-$ was confirmed by LC-MS analysis (Scheme S3, Figures S24 and S25). A 488 nm excitation wavelength was used for the measurements in aqueous solution since it was the excitation wavelength for cellular imaging experiments (green channel, $\lambda_{em}$ = 500−575 nm, $\lambda_{ex}$ = 488 nm).

Subsequently we evaluated the ability of ATP-LW to detect ATP. A large increase in fluorescence intensity at 587 nm (>80-fold, see Figure 1c and Figure S4) was observed following the addition of ATP (0−15 mM) to an aqueous solution of ATP-LW when the samples were excited at 520 nm. However, the addition of ATP (0−15 mM) to ATP-LW resulted in only a small increase in the fluorescence intensity upon excitation at either 450 (Figure 1d) or 488 nm (Figure S6). The disparity in emission and excitation profiles seen for ATP and $ONOO^-$ provides support for the notion that ATP-LW may be used to detect separately, albeit contemporaneously, these two important analytes.

We then explored the fluorescence response of ATP-LW in the presence of both $ONOO^-$ and ATP. It was found that the peak at 589 nm for ATP-LW retained sensitivity to changes in the ATP concentration even after the addition of $ONOO^-$ (16 $\mu$M) when excitation was effected at 520 nm (Figure S13). Conversely, the emission peaks at 562 nm (Figure S14) or 569 nm (Figure S15) were seen to change as a function of the $ONOO^-$ concentration, but were only slightly influenced by the presence or absence of ATP (15 mM). These results were taken as a further indication that ATP-LW may be used to detect $ONOO^-$ and ATP independently, on the condition that two different excitation wavelengths are used (Scheme 1). We appreciate that the two emission peaks for ATP-LW are not well separated. As such, it is difficult to ascertain whether Förster resonance energy transfer (FRET) is occurring between the naphthalimide and rhodamine that make up ATP-LW.[39] However, on the basis of density functional theoretical analysis we believe that FRET does not occur to a significant extent between the two fluorophores present in ATP-LW (Figure S22).

We then evaluated the selectivity of the probe ATP-LW toward a variety of potential biologically relevant interferents (Figures 2 and 3). Other ROS, such as $H_2O_2$ and HOCl, led to no change in the fluorescence intensity of ATP-LW under conditions identical to those used to study $ONOO^-$ and ATP (Figure 2). However, exposure of ATP-LW to ADP (10 mM) led to an enhancement in the fluorescence intensity (Figure 3). Since the concentration of ATP is around 1000-fold higher than ADP in cells,[3] as noted above, it seems highly unlikely

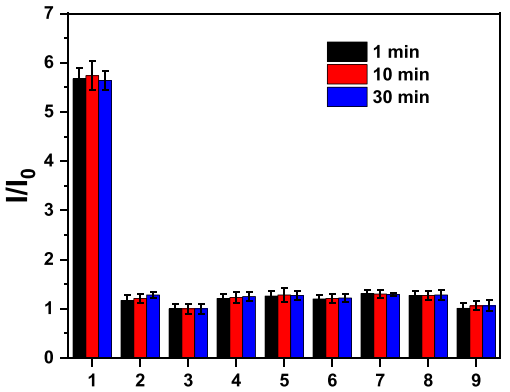


**Figure 2.** Selectivity bar chart for probe ATP-LW (15 $\mu$M) in PBS buffer solution (10 mM, v/v, $EtOH/H_2O$ = 1/99, pH = 7.40) with $ONOO^-$ (16 $\mu$M) or other ROS. (1) $ONOO^-$; (2) $H_2O_2$ (100 $\mu$M); (3) probe ATP-LW alone; (4) HOCl (100 $\mu$M); (5) $ROO^\bullet$ (200 $\mu$M); (6) $^\bullet OH$ (100 $\mu$M); (7) $O_2^{\bullet-}$ (100 $\mu$M); (8) $^1O_2$ (100 $\mu$M); (9) APAP (20 mM); $\lambda_{ex/em}$= 450 (bandwidth 8) nm/562 nm. Time points were taken at 1 min (black bars), 10 min (red bars), and 30 min (blue bars).

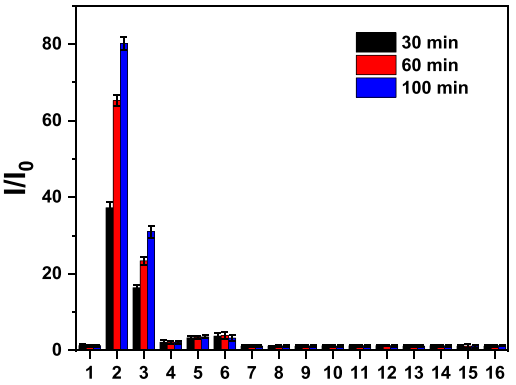


**Figure 3.** Selectivity bar chart of ATP-LW (15 $\mu$M) in PBS buffer solution (10 mM, v/v, $EtOH/H_2O$ = 1/99, pH = 7.40) upon treatment with ATP (15 mM) or other potential interferents. (1) Probe ATP-LW alone; (2) ATP (15 mM); (3) adenosine diphosphate (ADP, 10 mM); (4) uridine 5′-triphosphate, trisodium salt (UTP trisodium salt 10 mM); (5) guanosine 5′-triphosphate, disodium salt (GTP disodium salt, 10 mM); (6) cytidine 5′-triphosphate disodium salt (CTP disodium salt, 10 mM); (7) cysteine (1 mM); (8) glutathione (1 mM); (9) homocysteine (1 mM); (10) KCl (6 mM); (11) $CaCl_2$ (2 mM); (12) $MgCl_2$ (1 mM); (13) $CuCl_2$ (100 $\mu$M); (14) $ZnCl_2$ (100 $\mu$M); (15) NaCl (100 mM); (16) APAP (20 mM); $\lambda_{ex/em}$ = 520 (bandwidth 8) nm/587 nm. Time points were taken at 30 min (black bars), 60 min (red bars), and 100 min (blue bars).

that this cross reactivity will preclude the use of ATP-LW for the effective detection of ATP in cells.

Exposure to $ONOO^-$ resulted in a statistically significant fluorescence increase that was instantaneous on the laboratory time scale (Figure S16), while the reaction of ATP-LW and ATP required approximately 100 min to reach saturation (Figure S17). We next confirmed that ATP-LW exhibits good stability over a pH range from 3 to 11 (Figures S11 and S12). The fluorescence emission of a test solution formed by treating ATP-LW with $ONOO^-$ was found to decrease at lower pH, a finding that could reflect the known decomposition of $ONOO^-$ in acidic media (Figure S11).[41] The fluorescence intensity at 587 nm was also found to decrease at higher pH



https://doi.org/10.1021/jacs.1c07954
J. Am. Chem. Soc. 2022, 144, 174−183

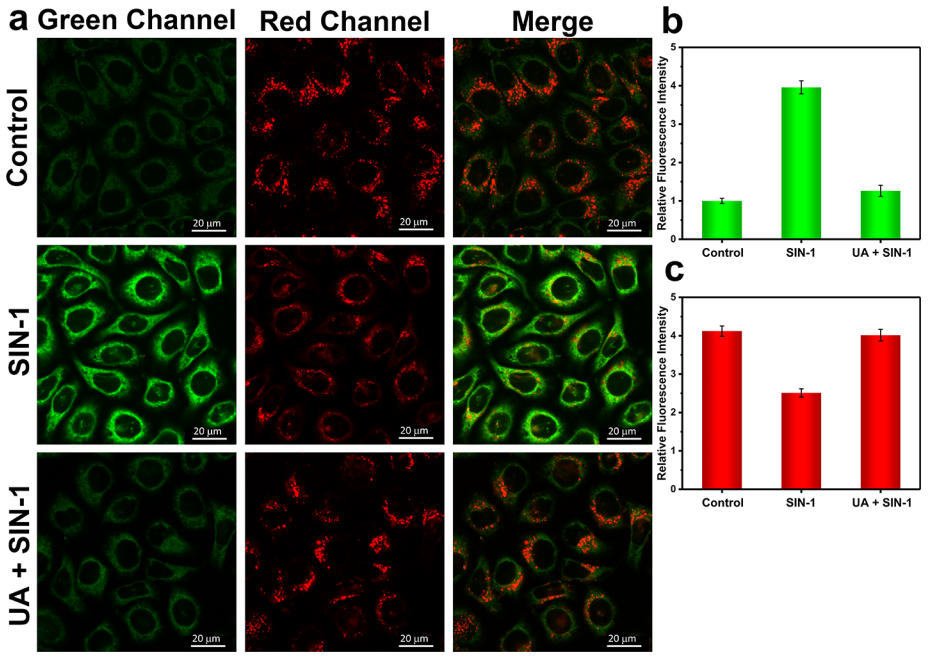


**Figure 4.** One-photon confocal imaging of $ONOO^-$ and ATP levels in hepatocytes treated with SIN-1 or SIN-1/uric acid. (a) One-photon fluorescence images of HL-7702 cells recorded after the addition of SIN-1 (1 mM, 1 h) and uric acid (500 $\mu$M, 1 h) with monitoring over the green ($ONOO^-$) and red (ATP) channels. Control group: Cells were stained with probe ATP-LW (20 $\mu$M) for 20 min. SIN-1 group: Cells were incubated with SIN-1 (1 mM) for 1 h, then stained with probe ATP-LW (20 $\mu$M) for 20 min. UA + SIN-1 group: Cells were pretreated with uric acid (500 $\mu$M) for 1 h and followed by adding SIN-1 (1 mM) for 1 h and then stained with probe ATP-LW (20 $\mu$M) for 20 min. Green fluorescence channel for $ONOO^-$: $\lambda_{ex}$ = 488 nm, $\lambda_{em}$ = 500−575 nm. Red fluorescence channel for ATP: $\lambda_{ex}$ = 514 nm, $\lambda_{em}$ = 575−650 nm. (b) Green relative fluorescence intensity output of three groups. (c) Red relative fluorescence intensity output of three groups. Note: The green fluorescence intensity of the control group is defined as 1.0. The data are expressed as the mean ± SD. Concordant results were obtained from five independent experiments.

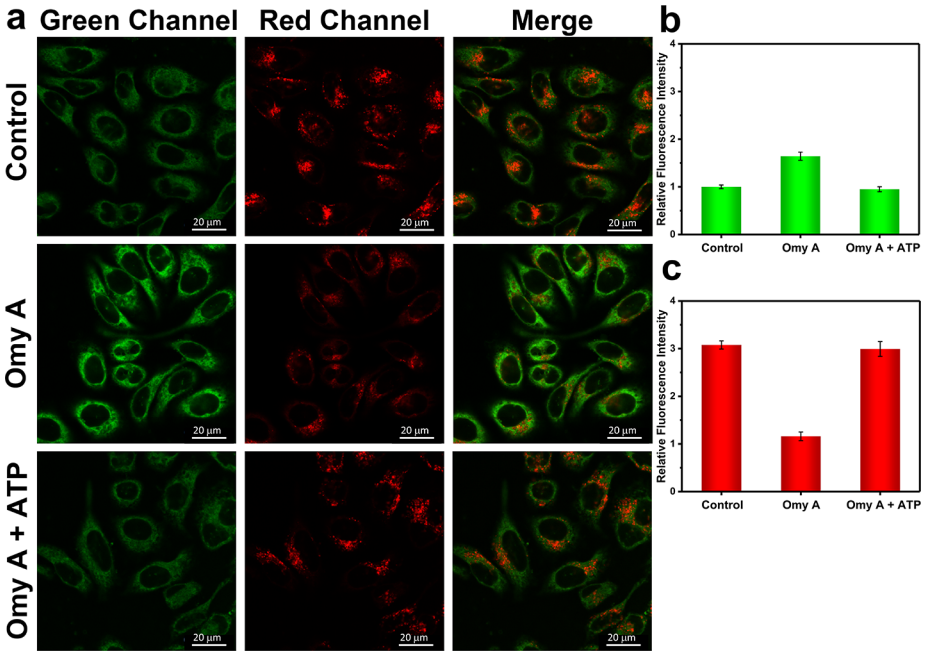


**Figure 5.** One-photon confocal imaging of $ONOO^-$ and ATP levels in hepatocytes treated with omy A or omy A/ATP. (a) One-photon fluorescence images of HL-7702 cells with the addition of omy A (25 $\mu$M, 1 h) and ATP (10 mM, 1 h) for green ($ONOO^-$) and red (ATP) channels. Control group: Cells were stained with probe ATP-LW (20 $\mu$M) for 20 min. Omy A group: Cells were incubated with omy A (25 $\mu$M) for 1 h, then stained with probe ATP-LW (20 $\mu$M) for 20 min. Omy A + ATP group: Cells were pretreated with omy A (25 $\mu$M) for 1 h followed by adding ATP (10 mM) for 1 h and then stained with probe ATP-LW (20 $\mu$M) for 20 min. Green fluorescence channel for $ONOO^-$: $\lambda_{ex}$ = 488 nm, $\lambda_{em}$ = 500−575 nm. Red fluorescence channel for ATP: $\lambda_{ex}$ = 514 nm, $\lambda_{em}$ = 575−650 nm. (b) Green relative fluorescence intensity output of three groups. (c) Red relative fluorescence intensity output of three groups. Note: The green fluorescence intensity of the control group is defined as 1.0. The data are expressed as the mean ± SD. Concordant results were obtained from five independent experiments.



https://doi.org/10.1021/jacs.1c07954
J. Am. Chem. Soc. 2022, 144, 174−183

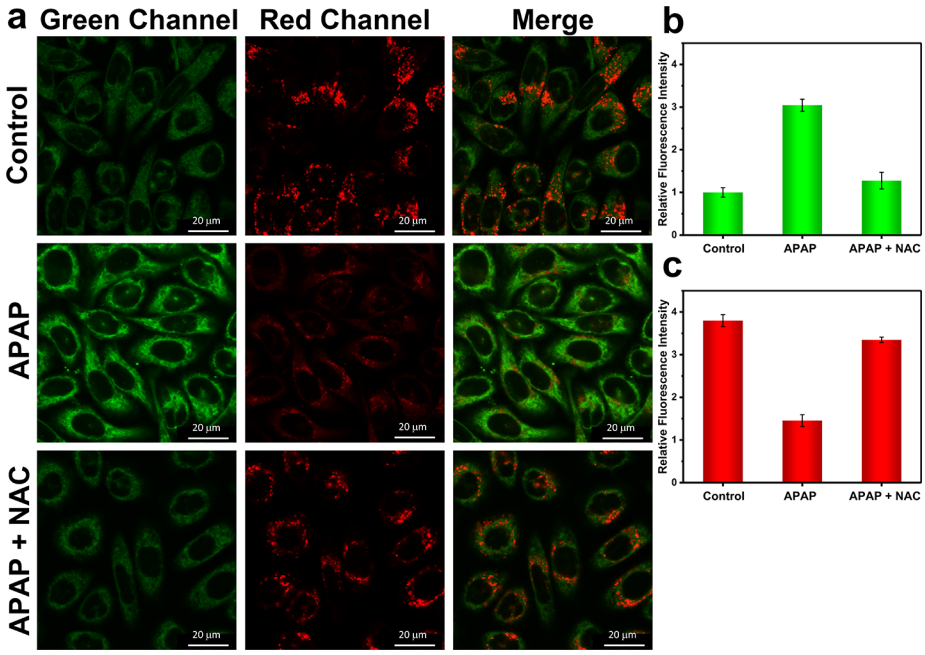


**Figure 6.** One-photon confocal images of APAP-induced injury and its remediation by NAC in HL-7702 cells. (a) One-photon fluorescence images of HL-7702 cells with the addition of APAP (15 mM, 2 h) and NAC (2 mM, 2 h) for green ($ONOO^-$) and red (ATP) channels. Control group: Cells were stained with probe ATP-LW (20 $\mu$M) for 20 min. APAP group: Cells were incubated with APAP (15 mM) for 2 h and then stained with probe ATP-LW (20 $\mu$M) for 20 min. APAP + NAC group: Cells were pretreated with NAC (2 mM) for 2 h and then incubated with APAP (15 mM) for 2 h, followed by staining with probe ATP-LW (20 $\mu$M) for another 20 min. Green fluorescence channel for $ONOO^-$: $\lambda_{ex}$ = 488 nm, $\lambda_{em}$ = 500−575 nm. Red fluorescence channel for ATP: $\lambda_{ex}$ = 514 nm, $\lambda_{em}$ = 575−650 nm. (b) Green relative fluorescence intensity output of three groups. (c) Red relative fluorescence intensity output of three groups. Note: The green fluorescence intensity of the control group is defined as 1.0. The data are expressed as the mean ± SD. Concordant results were obtained from five independent experiments.

(pH > 8), a result ascribed to the hydrolysis of ATP under basic conditions (Figure S12).[42]

The above results prompted us to explore the use of ATP-LW for imaging live cells. First, we confirmed using an MTT assay that ATP-LW was non-toxic to HL-7702 cells over concentrations ranging from 0 to 1 mM with an incubation time of 24 h (Figure S27). The ability of ATP-LW to image $ONOO^-$ and ATP in living cells was then evaluated using excitation wavelengths of 488 and 514 nm, respectively. ATP-LW demonstrated a clear "turn on" response upon the addition of 3-morpholinosydnonimine hydrochloride (SIN-1, a donor of $ONOO^-$)[43] when monitored using the green channel (Figure 4a and b). Meanwhile, a 0.61-fold decrease in the red channel was observed as compared to the control group (Figure 4c). We then evaluated crosstalk between the two channels, and as expected, no appreciable fluorescence was observed in either channel 3 ($\lambda_{ex}$ = 488 nm, $\lambda_{em}$ = 575−650 nm) or channel 4 ($\lambda_{ex}$ = 514 nm, $\lambda_{em}$ = 520−575 nm) when HL-7702 cells were treated with ATP-LW and simultaneously exposed to ATP and SIN-1 (Figure S28). Having confirmed the absence of crosstalk, fluorescence changes using the $ONOO^-$ scavenger uric acid were evaluated.[44] The addition of uric acid (500 $\mu$M) and SIN-1 (1.0 mM) led to a 0.32-fold decrease in the average green fluorescence intensity and 1.60-fold enhancement in the average red fluorescence intensity, when compared with the corresponding SIN-1 group (as determined by monitoring the green and red channels, respectively, Figure 4). These results are consistent with suggestions in the literature that an increase in the $ONOO^-$ concentration can result in depletion of ATP.[22]

We then set out to evaluate how imbalances in the energy metabolism instigated by obstructing ATP production can influence production of $ONOO^-$. Oligomycin A (omy A) inhibits ATP synthase by blocking its $F_O$ unit.[45] As shown in Figure 5, after hepatocytes were incubated with omy A (25 $\mu$M) for 1 h, a 38% decrease in the red channel signal relative to the initial level was seen (Figure 5c). Concurrently, a 1.64-fold increase in the green channel intensity was seen, as expected for an increase in the $ONOO^-$ levels as compared to healthy hepatocytes (Figure 5b). The addition of exogenous ATP (10 mM) yielded a green channel intensity that was 95% of the control group (Figure 5b), while the intensity of the red channel increased to almost the same level as the control group (Figure 5c). While not a proof, these findings support the conclusion that the addition of exogenous ATP induces recovery[26] and that ROS/RNS production is affected by mitochondrial damage to ATP synthesis, leading to an increase of $ONOO^-$. These results are not surprising since it is known that omy A induces cellular apoptosis via ATP inhibition;[46,47] moreover, oxidative stress (i.e., $ONOO^-$) is an associated factor in apoptosis-related cell death.[48] As such, our results support the conclusion that omy A induces the production of $ONOO^-$ in a cellular environment via ATP inhibition.

ROS and RNS are regarded as biomarkers in DILI and are thus analytes that have been frequently targeted using fluorescent probes.[19,21] Previous studies confirm that ATP production is decreased by exposure to APAP.[22,49,50] APAP-induced hepatoxicity was thus chosen as the model to investigate whether ATP-LW could detect $ONOO^-$ and ATP, since these two species could serve as early diagnostic biomarkers. Treatment of HL-7702 cells with APAP produced a marked increase in the fluorescence of the green channel and a significant decrease in the fluorescence in the red channel (Figure 6). This finding underscores how upregulation of


https://doi.org/10.1021/jacs.1c07954
J. Am. Chem. Soc. 2022, 144, 174−183

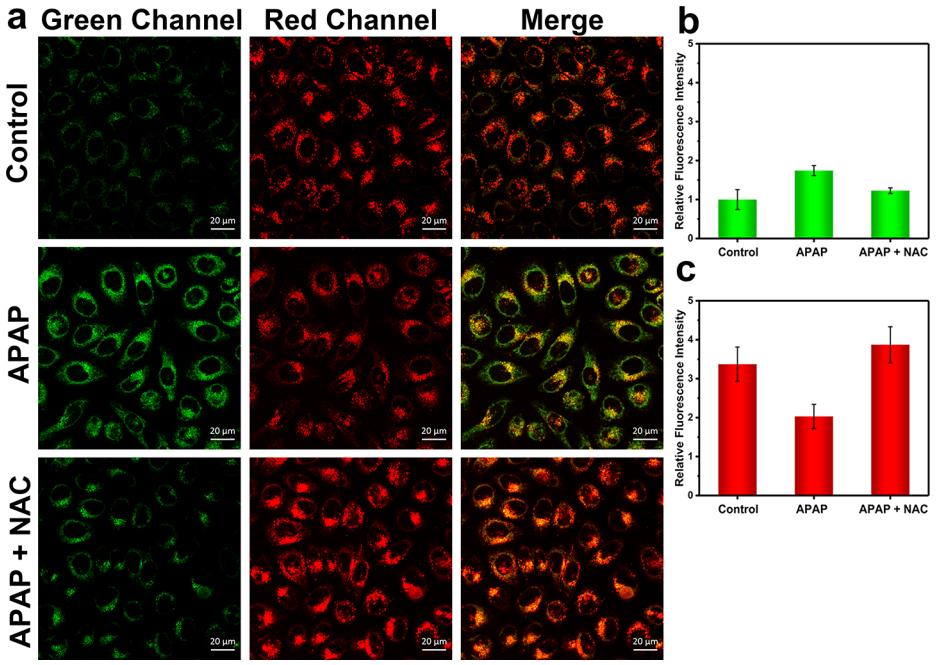


**Figure 7.** Two-photon fluorescence images of APAP-induced injury with HL-7702 cells. (a) Two-photon fluorescence images of HL-7702 cells with the addition of APAP (20 mM, 2 h) and NAC (2 mM, 2 h) for green ($ONOO^-$) and red (ATP) channels. Control group: Cells were stained with probe ATP-LW (20 $\mu$M) for 20 min. APAP group: Cells were incubated with APAP (20 mM) for 2 h and then stained with probe ATP-LW (20 $\mu$M) for 20 min. APAP + NAC group: Cells were pretreated with NAC (2 mM) for 2 h and then incubated with APAP (20 mM) for 2 h, followed by staining with probe ATP-LW (20 $\mu$M) for another 20 min. Two-photon green fluorescence channel for $ONOO^-$: $\lambda_{ex}$ = 976 nm, $\lambda_{em}$ = 500−575 nm. Two-photon red fluorescence channel for ATP: $\lambda_{ex}$ = 1028 nm, $\lambda_{em}$ = 575−680 nm. (b) Green relative fluorescence intensity output of three groups. (c) Red relative fluorescence intensity output of three groups. Note: The green fluorescence intensity of the control group is defined as 1.0. The data are expressed as the mean ± SD. Concordant results were obtained from five independent experiments.

intracellular $ONOO^-$ and depletion of ATP occur after administration of APAP while serving to illustrate the ability of our probe to detect concentration changes of these two biomarkers via one-photon confocal imaging in a DILI cellular model. This was further confirmed using *N*-acetyl-L-cysteine (NAC), which is a precursor for the substrate (L-cysteine) in the synthesis of reduced glutathione (GSH) and commonly used for the treatment of APAP overdose.[51,52] GSH is capable of eliminating $ONOO^-$, and as such has been used to help treat APAP overdoses.[53,54] Upon addition of NAC, the fluorescence intensity in the green channel decreased and that of the red channel increased (Figure 6). This finding is thus consistent with the reduction of $ONOO^-$ and an increase in the ATP concentration under these conditions.

Our attention then turned to two-photon imaging[55] of $ONOO^-$ and ATP using ATP-LW, with the same cell models used above. The results (Figure 7) served to confirm the ability of ATP-LW to image both $ONOO^-$ and ATP, using an excitation of 976 nm for the former and 1028 nm for the latter, and we extended the emission range for the red channel (i.e., 575−680 nm).

## CONCLUSION

In summary, we have developed a novel dual-analyte fluorescent probe (ATP-LW), which provides a fluorescence response toward $ONOO^-$ and ATP simultaneously by means of different excitation wavelengths. Probe ATP-LW comprises two responsive units that are expected to react independently with $ONOO^-$ and ATP, respectively.[31] Upon the addition of $ONOO^-$ alone, the 4-hydroxy-1,8-naphthalimide subunit luminesces ($\lambda_{ex}$ = 450 nm, $\lambda_{em}$ = 562 nm or $\lambda_{ex}$ = 488 nm, $\lambda_{em}$ = 568 nm); conversely, when ATP alone is present, the rhodamine ring opens and luminesces ($\lambda_{ex}$ = 520 nm, $\lambda_{em}$ = 587 nm). In order to detect $ONOO^-$ and ATP in cellular milieus with minimal crosstalk, we choose to monitor the emission over the green channel ($\lambda_{ex}$ = 488 nm, $\lambda_{em}$ = 500−575 nm) and red channel ($\lambda_{ex}$ = 514 nm, $\lambda_{em}$ = 575−650 nm). It was found that by using ATP-LW and two different channels it is possible to monitor concurrently the enhancement of $ONOO^-$ and depletion of ATP during APAP-induced hepatotoxicity. This monitoring provides support for the proposed signaling pathways for APAP-induced toxicity wherein $ONOO^-$ increases and ATP depletion are thought to be responsible for hepatic necrosis.[56] We anticipate that ATP-LW can be extended to image fluctuations of these two biomarkers in other diseases, such as ischemia-reperfusion injury.[14]

## ASSOCIATED CONTENT

### Supporting Information

The Supporting Information is available free of charge at https://pubs.acs.org/doi/10.1021/jacs.1c07954.

Materials and instruments used; mechanism of APAP-induced toxicity; synthesis and analysis of ATP-LW, including mass spectrometric analyses and NMR spectra; methods used for the generation of ROS/RNS; UV−vis and fluorescence analyses; theoretical calculations and transient absorption spectra; cell culture protocols; MTT assay and fluorescence imaging of live cells (PDF)



https://doi.org/10.1021/jacs.1c07954
J. Am. Chem. Soc. 2022, 144, 174−183

## AUTHOR INFORMATION


### Corresponding Authors

**Hai-Hao Han** − *Key Laboratory for Advanced Materials and Joint International Research Laboratory of Precision Chemistry and Molecular Engineering, Feringa Nobel Prize Scientist Joint Research Center, School of Chemistry and Molecular Engineering, East China University of Science and Technology, Shanghai 200237, People's Republic of China*; Email: hanhaihao@126.com

**Hua Zhang** − *School of Physics, Henan Normal University, Xinxiang 453007, People's Republic of China*; Email: zhanghua1106@163.com

**Chusen Huang** − *The Education Ministry Key Laboratory of Resource Chemistry, Shanghai Key Laboratory of Rare Earth Functional Materials, and Shanghai Municipal Education Committee Key Laboratory of Molecular Imaging Probes and Sensors, Department of Chemistry, Shanghai Normal University, Shanghai 200234, People's Republic of China*; orcid.org/0000-0002-2481-9147; Email: huangcs@shnu.edu.cn

**Ping Li** − *College of Chemistry, Chemical Engineering and Materials Science, Key Laboratory of Molecular and Nano Probes, Ministry of Education, Collaborative Innovation Center of Functionalized Probes for Chemical Imaging in Universities of Shandong, Institutes of Biomedical Sciences, Shandong Normal University, Jinan 250014, People's Republic of China*; orcid.org/0000-0002-2356-0962; Email: lip@sdnu.edu.cn

**Tony D. James** − *College of Chemistry, Chemical Engineering and Materials Science, Key Laboratory of Molecular and Nano Probes, Ministry of Education, Collaborative Innovation Center of Functionalized Probes for Chemical Imaging in Universities of Shandong, Institutes of Biomedical Sciences, Shandong Normal University, Jinan 250014, People's Republic of China; Department of Chemistry, University of Bath, Bath BA2 7AY, U.K.; School of Physics, Henan Normal University, Xinxiang 453007, People's Republic of China*; orcid.org/0000-0002-4095-2191; Email: t.d.james@bath.ac.uk

**Jonathan L. Sessler** − *Department of Chemistry, The University of Texas at Austin, Austin, Texas 78712-1224, United States*; orcid.org/0000-0002-9576-1325; Email: sessler@cm.utexas.edu

### Authors

**Luling Wu** − *College of Chemistry, Chemical Engineering and Materials Science, Key Laboratory of Molecular and Nano Probes, Ministry of Education, Collaborative Innovation Center of Functionalized Probes for Chemical Imaging in Universities of Shandong, Institutes of Biomedical Sciences, Shandong Normal University, Jinan 250014, People's Republic of China; The Education Ministry Key Laboratory of Resource Chemistry, Shanghai Key Laboratory of Rare Earth Functional Materials, and Shanghai Municipal Education Committee Key Laboratory of Molecular Imaging Probes and Sensors, Department of Chemistry, Shanghai Normal University, Shanghai 200234, People's Republic of China; Department of Chemistry, University of Bath, Bath BA2 7AY, U.K.*; orcid.org/0000-0001-6574-5861

**Jihong Liu** − *College of Chemistry, Chemical Engineering and Materials Science, Key Laboratory of Molecular and Nano Probes, Ministry of Education, Collaborative Innovation Center of Functionalized Probes for Chemical Imaging in Universities of Shandong, Institutes of Biomedical Sciences, Shandong Normal University, Jinan 250014, People's Republic of China*; orcid.org/0000-0003-3306-7802

**Xue Tian** − *Department of Chemistry, University of Bath, Bath BA2 7AY, U.K.*; orcid.org/0000-0002-9494-3493

**Robin R. Groleau** − *Department of Chemistry, University of Bath, Bath BA2 7AY, U.K.*

**Beidou Feng** − *School of Physics, Henan Normal University, Xinxiang 453007, People's Republic of China*

**Yonggang Yang** − *School of Physics, Henan Normal University, Xinxiang 453007, People's Republic of China*

**Adam C. Sedgwick** − *Department of Chemistry, The University of Texas at Austin, Austin, Texas 78712-1224, United States*; orcid.org/0000-0002-3132-2913

**Yang Wang** − *The Education Ministry Key Laboratory of Resource Chemistry, Shanghai Key Laboratory of Rare Earth Functional Materials, and Shanghai Municipal Education Committee Key Laboratory of Molecular Imaging Probes and Sensors, Department of Chemistry, Shanghai Normal University, Shanghai 200234, People's Republic of China*

**Han-Min Wang** − *National Center for Drug Screening, State Key Laboratory of Drug Research, Shanghai Institute of Materia Medica, Chinese Academy of Sciences, Shanghai 201203, People's Republic of China*

**Fang Huang** − *College of Chemistry, Chemical Engineering and Materials Science, Key Laboratory of Molecular and Nano Probes, Ministry of Education, Collaborative Innovation Center of Functionalized Probes for Chemical Imaging in Universities of Shandong, Institutes of Biomedical Sciences, Shandong Normal University, Jinan 250014, People's Republic of China*; orcid.org/0000-0003-4801-7111

**Steven D. Bull** − *Department of Chemistry, University of Bath, Bath BA2 7AY, U.K.*; orcid.org/0000-0001-8244-5123

**Yi Zang** − *National Center for Drug Screening, State Key Laboratory of Drug Research, Shanghai Institute of Materia Medica, Chinese Academy of Sciences, Shanghai 201203, People's Republic of China*

**Jia Li** − *National Center for Drug Screening, State Key Laboratory of Drug Research, Shanghai Institute of Materia Medica, Chinese Academy of Sciences, Shanghai 201203, People's Republic of China*

**Xiao-Peng He** − *Key Laboratory for Advanced Materials and Joint International Research Laboratory of Precision Chemistry and Molecular Engineering, Feringa Nobel Prize Scientist Joint Research Center, School of Chemistry and Molecular Engineering, East China University of Science and Technology, Shanghai 200237, People's Republic of China*; orcid.org/0000-0002-8736-3511

**Bo Tang** − *College of Chemistry, Chemical Engineering and Materials Science, Key Laboratory of Molecular and Nano Probes, Ministry of Education, Collaborative Innovation Center of Functionalized Probes for Chemical Imaging in Universities of Shandong, Institutes of Biomedical Sciences, Shandong Normal University, Jinan 250014, People's Republic of China*; orcid.org/0000-0002-8712-7025

Complete contact information is available at: https://pubs.acs.org/10.1021/jacs.1c07954


### Author Contributions

‡L.W., J.L., and X.T. contributed equally.



https://doi.org/10.1021/jacs.1c07954
J. Am. Chem. Soc. 2022, 144, 174−183

### Notes

The authors declare no competing financial interest.

## ■ ACKNOWLEDGMENTS

L.W. wishes to thank China Scholarship Council and the University of Bath for supporting his Ph.D. in the UK. R.R.G. wishes to thank the EPSRC Centre for Doctoral Training in Catalysis (EP/L016443/1). We would like to thank the EPSRC and the University of Bath for funding. T.D.J. wishes to thank the Royal Society for a Wolfson Research Merit Award and the Open Research Fund of the School of Chemistry and Chemical Engineering, Henan Normal University, for support (2020ZD01). P.L. and B.T. thank the National Natural Science Foundation of China (21927811, 22074083), the Key Research and Development Program of Shandong Province (2018YFJH0502), and the National Science Foundation of Shandong Province of China (ZR2020ZD17). C.H. thanks the National Natural Science Foundation of China (Grants 21672150, 21302125), Alexander von Humboldt Foundation (AvH), Shanghai Rising-Star Program (19QA1406400), and the Shanghai Government (18DZ2254200). H.-H.H. would like to thank the Project funded by China Postdoctoral Science Foundation (No. 2020M681196). X.-P.H. thanks the National Natural Science Foundation (No. 91853201), the Shanghai Municipal Science and Technology Major Project (2018SHZDZX03), the National Key Sci-Tech Special Projects of Infection Diseases of China (2018ZX10732202), and the International Cooperation Program of Shanghai Science and Technology Committee (17520750100). H.Z. thanks the National Natural Science Foundation of China (21722501, 11974103), the Zhongyuan High Level Talents Special Support Plan—Science and Technology Innovation Leading Talents (204200510006), and Program for Science Technology Innovation Talents in Universities of Henan Province (21HASTIT019). J.L.S. thanks the Robert A. Welch Foundation (F-0018) for support. NMR spectroscopic and mass spectrometric services were provided by the Material and Chemical Characterisation Facility ($MC^2$) at the University of Bath (http://go.bath.ac.uk/mc2), and we would like to thank Dr. John Lowe for his support with characterization. We are also grateful to Feng-Ming Liu, Yao Li, and Yang Yu from the National Facility for Protein Science in Shanghai (NFPS) for their kind discussions on preliminary bioimaging experiments.

## ■ REFERENCES

(1) Knowles, J. R. Enzyme-catalyzed phosphoryl transfer reactions. *Annu. Rev. Biochem.* **1980**, *49*, 877−919.
(2) Higgins, C. F.; Hiles, I. D.; Salmond, G. P. C.; Gill, D. R.; Downie, J. A.; Evans, I. J.; Holland, I. B.; Gray, L.; Buckel, S. D.; Bell, A. W.; Hermodson, M. A. A family of related ATP-binding subunits coupled to many distinct biological processes in bacteria. *Nature* **1986**, *323*, 448−450.
(3) Zimmerman, J. J.; von Saint André-von Arnim, A.; McLaughlin, J. In *Pediatric Critical Care*, 4th ed.; Fuhrman, B. P.; Zimmerman, J. J., Eds.; Mosby, 2011; Chapter 74, pp 1058−1072.
(4) Davalos, D.; Grutzendler, J.; Yang, G.; Kim, J. V.; Zuo, Y.; Jung, S.; Littman, D. R.; Dustin, M. L.; Gan, W.-B. ATP mediates rapid microglial response to local brain injury in vivo. *Nat. Neurosci.* **2005**, *8*, 752−758.
(5) Burnstock, G. Historical review: ATP as a neurotransmitter. *Trends Pharmacol. Sci.* **2006**, *27*, 166−176.
(6) Ashcroft, F. M.; Gribble, F. M. ATP-sensitive $K^+$ channels and insulin secretion: their role in health and disease. *Diabetologia* **1999**, *42*, 903−919.
(7) Bush, K. T.; Keller, S. H.; Nigam, S. K. Genesis and reversal of the ischemic phenotype in epithelial cells. *J. Clin. Invest.* **2000**, *106*, 621−626.
(8) Lee, S. J.; Jin, Y.; Yoon, H. Y.; Choi, B.-O.; Kim, H. C.; Oh, Y.-K.; Kim, H.-S.; Kim, W.-K. Ciclopirox protects mitochondria from hydrogen peroxide toxicity. *Br. J. Pharmacol.* **2005**, *145*, 469−476.
(9) Radi, R.; Cassina, A.; Hodara, R.; Quijano, C.; Castro, L. Peroxynitrite reactions and formation in mitochondria. *Free Radical Biol. Med.* **2002**, *33*, 1451−1464.
(10) Szabó, C.; Ischiropoulos, H.; Radi, R. Peroxynitrite: biochemistry, pathophysiology and development of therapeutics. *Nat. Rev. Drug Discovery* **2007**, *6*, 662−680.
(11) Valez, V.; Cassina, A.; Batinic-Haberle, I.; Kalyanaraman, B.; Ferrer-Sueta, G.; Radi, R. Peroxynitrite formation in nitric oxide-exposed submitochondrial particles: Detection, oxidative damage and catalytic removal by Mn-porphyrins. *Arch. Biochem. Biophys.* **2013**, *529*, 45−54.
(12) Uribe, P.; Treulen, F.; Boguen, R.; Sánchez, R.; Villegas, J. V. Nitrosative stress by peroxynitrite impairs ATP production in human spermatozoa. *Andrologia* **2017**, *49*, e12615.
(13) Graves, J. E.; Lewis, S. J.; Kooy, N. W. Role of ATP-sensitive $K^+$-channels in hemodynamic effects of peroxynitrite in anesthetized rats. *J. Cardiovasc. Pharmacol.* **2005**, *46*, 653−659.
(14) Nilakantan, V.; Liang, H.; Maenpaa, C. J.; Johnson, C. P. Differential patterns of peroxynitrite mediated apoptosis in proximal tubular epithelial cells following ATP depletion recovery. *Apoptosis* **2008**, *13*, 621−633.
(15) Wang, S.; Chen, L.; Jangili, P.; Sharma, A.; Li, W.; Hou, J.-T.; Qin, C.; Yoon, J.; Kim, J. S. Design and applications of fluorescent detectors for peroxynitrite. *Coord. Chem. Rev.* **2018**, *374*, 36−54.
(16) Jiao, X.; Li, Y.; Niu, J.; Xie, X.; Wang, X.; Tang, B. Small-molecule fluorescent probes for imaging and detection of reactive oxygen, nitrogen, and sulfur species in biological systems. *Anal. Chem.* **2018**, *90*, 533−555.
(17) Xiong, J.; Wang, W.; Wang, C.; Zhong, C.; Ruan, R.; Mao, Z.; Liu, Z. Visualizing peroxynitrite in microvessels of the brain with stroke using an engineered highly specific fluorescent probe. *ACS Sen.* **2020**, *5*, 3237−3245.
(18) Jun, Y. W.; Sarkar, S.; Kim, K. H.; Ahn, K. H. Molecular probes for fluorescent imaging of ATP in cell and tissue. *ChemPhotoChem* **2019**, *3*, 214−219.
(19) Chen, J.; Huang, D.; She, M.; Wang, Z.; Chen, X.; Liu, P.; Zhang, S.; Li, J. Recent progress in fluorescent sensors for drug-induced liver injury assessment. *ACS Sens.* **2021**, *6*, 628−640.
(20) Wu, L.; Liu, J.; Tian, X.; Groleau, R. R.; Bull, S. D.; Li, P.; Tang, B.; James, T. D. Fluorescent probe for the imaging of superoxide and peroxynitrite during drug-induced liver injury. *Chem. Sci.* **2021**, *12*, 3921−3928.
(21) Cheng, D.; Xu, W.; Gong, X.; Yuan, L.; Zhang, X.-B. Design strategy of fluorescent probes for live drug-induced acute liver injury imaging. *Acc. Chem. Res.* **2021**, *54*, 403−415.
(22) Maruf, A. A.; Lee, O.; O'Brien, P. J. Modifications of Mitochondrial Function by Toxicants. In *Reference Module in Biomedical Sciences*; Elsevier, 2014.
(23) Masubuchi, Y.; Suda, C.; Horie, T. Involvement of mitochondrial permeability transition in acetaminophen-induced liver injury in mice. *J. Hepatol.* **2005**, *42*, 110−116.
(24) Sen, S.; Hufnagel, S.; Maier, E. Y.; Aguilar, I.; Selvakumar, J.; DeVore, J. E.; Lynch, V. M.; Arumugam, K.; Cui, Z.; Sessler, J. L.; Arambula, J. F. Rationally designed redox-active Au (I) N-heterocyclic carbene: an immunogenic cell death inducer. *J. Am. Chem. Soc.* **2020**, *142*, 20536−20541.
(25) Wu, L.; Han, H.-H.; Wang, Y.; Tian, X.; Bull, S. D.; Sedgwick, A. C.; He, X.-P.; Huang, C.; James, T. D.; Sessler, J. L. Dual-function fluorescent probe for the detection of peroxynitrite and adenosine

triphosphate. *ChemRxiv*, **2019** DOI: 10.26434/chemrxiv.7777112.v1 (accessed 2021−11−25).
(26) Wu, Z.; Liu, M.; Liu, Z.; Tian, Y. Real-time imaging and simultaneous quantification of mitochondrial $H_2O_2$ and ATP in neurons with a single two-photon fluorescence-lifetime-based probe. *J. Am. Chem. Soc.* **2020**, *142*, 7532−7541.
(27) Merck, https://www.merckmillipore.com/GB/en/product/BioTracker-ATP-LW-Live-Cell-Dye,MM_NF-SCT069 (accessed 2021−11−25).
(28) Sikora, A.; Zielonka, J.; Lopez, M.; Joseph, J.; Kalyanaraman, B. Direct oxidation of boronates by peroxynitrite: mechanism and implications in fluorescence imaging of peroxynitrite. *Free Radical Biol. Med.* **2009**, *47*, 1401−1407.
(29) Sedgwick, A. C.; Han, H.-H.; Gardiner, J. E.; Bull, S. D.; He, X.-P.; James, T. D. Long-wavelength fluorescent boronate probes for the detection and intracellular imaging of peroxynitrite. *Chem. Commun.* **2017**, *53*, 12822−12825.
(30) Wu, L.; Tian, X.; Han, H.-H.; Wang, J.; Groleau, R. R.; Tosuwan, P.; Wannalerse, B.; Sedgwick, A. C.; Bull, S. D.; He, X.-P.; James, T. D. A simple near-infrared fluorescent probe for the detection of peroxynitrite. *ChemistryOpen* **2019**, *8*, 1407−1409.
(31) Wu, L.; Huang, J.; Pu, K.; James, T. D. Dual-locked spectroscopic probes for sensing and therapy. *Nat. Rev. Chem.* **2021**, *5*, 406−421.
(32) Erbas-Cakmak, S.; Kolemen, S.; Sedgwick, A. C.; Gunnlaugsson, T.; James, T. D.; Yoon, J.; Akkaya, E. U. Molecular logic gates: the past, present and future. *Chem. Soc. Rev.* **2018**, *47*, 2228−2248.
(33) de Silva, P. A.; Gunaratne, N. H. Q.; McCoy, C. P. A molecular photoionic AND gate based on fluorescent signalling. *Nature* **1993**, *364*, 42−44.
(34) Sedgwick, A. C.; Han, H.-H.; Gardiner, J. E.; Bull, S. D.; He, X.-P.; James, T. D. The development of a novel AND logic based fluorescence probe for the detection of peroxynitrite and GSH. *Chem. Sci.* **2018**, *9*, 3672−3676.
(35) Tian, X.; Kumawat, L. K.; Bull, S. D.; Elmes, R. B. P.; Wu, L.; James, T. D. Coumarin-based fluorescent probe for the detection of glutathione and nitroreductase. *Tetrahedron* **2021**, *82*, 131890.
(36) Wu, L.; Tian, X.; Groleau, R. R.; Wang, J.; Han, H.-H.; Reeksting, S. B.; Sedgwick, A. C.; He, X.-P.; Bull, S. D.; James, T. D. Coumarin-based fluorescent probe for the rapid detection of peroxynitrite 'AND' biological thiols. *RSC Adv.* **2020**, *10*, 13496−13499.
(37) Wu, L.; Gardiner, J. E.; Kumawat, L. K.; Han, H.-H.; Guo, R.; Li, X.; He, X.-P.; Elmes, R. B. P.; Sedgwick, A. C.; Bull, S. D.; James, T. D. Coumarin-based fluorescent 'AND' logic gate probes for the detection of homocysteine and a chosen biological analyte. *RSC Adv.* **2019**, *9*, 26425−26428.
(38) Wu, L.; Han, H.-H.; Liu, L.; Gardiner, J. E.; Sedgwick, A. C.; Huang, C.; Bull, S. D.; He, X.-P.; James, T. D. ESIPT-based fluorescence probe for the rapid detection of peroxynitrite 'AND' biological thiols. *Chem. Commun.* **2018**, *54*, 11336−11339.
(39) Fang, Y.; Shi, W.; Hu, Y.; Li, X.; Ma, H. A dual-function fluorescent probe for monitoring the degrees of hypoxia in living cells via the imaging of nitroreductase and adenosine triphosphate. *Chem. Commun.* **2018**, *54*, 5454−5457.
(40) Liang, X.; Xu, X.; Qiao, D.; Yin, Z.; Shang, L. Dual mechanism of an intramolecular charge transfer (ICT)-FRET-based fluorescent probe for the selective detection of hydrogen peroxide. *Chem. - Asian J.* **2017**, *12*, 3187−3194.
(41) Kirsch, M.; Korth, H.-G.; Wensing, A.; Sustmann, R.; de Groot, H. Product formation and kinetic simulations in the pH range 1−14 account for a free-radical mechanism of peroxynitrite decomposition. *Arch. Biochem. Biophys.* **2003**, *418*, 133−150.
(42) Phillips, R. C.; George, P.; Rutman, R. J. Thermodynamic data for the hydrolysis of adenosine triphosphate as a function of pH, $Mg^{2+}$ ion concentration, and ionic strength. *J. Biol. Chem.* **1969**, *244*, 3330−3342.
(43) Martin-Romero, F. J.; Gutiérrez-Martin, Y.; Henao, F.; Gutiérrez-Merino, C. Fluorescence measurements of steady state peroxynitrite production upon SIN-1 decomposition: NADH versus dihydrodichlorofluorescein and dihydrorhodamine 123. *J. Fluoresc.* **2004**, *14*, 17−23.
(44) Hooper, D. C.; Spitsin, S.; Kean, R. B.; Champion, J. M.; Dickson, G. M.; Chaudhry, I.; Koprowski, H. Uric acid, a natural scavenger of peroxynitrite, in experimental allergic encephalomyelitis and multiple sclerosis. *Proc. Natl. Acad. Sci. U. S. A.* **1998**, *95*, 675−680.
(45) Symersky, J.; Osowski, D.; Walters, D. E.; Mueller, D. M. Oligomycin frames a common drug-binding site in the ATP synthase. *Proc. Natl. Acad. Sci. U. S. A.* **2012**, *109*, 13961−13965.
(46) Wang, L.; Lu, D.; Huo, M.; Xu, H. Oligomycin A induces apoptosis-to-pyroptosis switch against melanoma with sensitized immunotherapy. *Adv. Funct. Mater.* **2021**, 2106332.
(47) Marton, A.; Mihalik, R.; Bratincsák, A.; Adleff, V.; Peták, I.; Végh, M.; Bauer, P. I.; Krajcsi, P. Apoptotic Cell death induced by inhibitors of energy conservation: Bcl-2 inhibits apoptosis downstream of a fall of ATP level. *Eur. J. Biochem.* **1997**, *250*, 467−475.
(48) Redza-Dutordoir, M.; Averill-Bates, D. A. Activation of apoptosis signalling pathways by reactive oxygen species. *Biochim. Biophys. Acta, Mol. Cell Res.* **2016**, *1863*, 2977−2992.
(49) Jaeschke, H.; Duan, L.; Nguyen, N. T.; Ramachandran, A. Mitochondrial damage and biogenesis in acetaminophen-induced liver injury. *Liver Res.* **2019**, *3*, 150−156.
(50) Lee, K. K.; Imaizumi, N.; Chamberland, S. R.; Alder, N. N.; Boelsterli, U. A. Targeting mitochondria with methylene blue protects mice against acetaminophen-induced liver injury. *Hepatology* **2015**, *61*, 326−336.
(51) Rushworth, G. F.; Megson, I. L. Existing and potential therapeutic uses for N-acetylcysteine: The need for conversion to intracellular glutathione for antioxidant benefits. *Pharmacol. Ther.* **2014**, *141*, 150−159.
(52) Wang, H.; Zhang, R.; Bridle, K. R.; Jayachandran, A.; Thomas, J. A.; Zhang, W.; Yuan, J.; Xu, Z. P.; Crawford, D. H. G.; Liang, X.; Liu, X.; Roberts, M. S. Two-photon dual imaging platform for in vivo monitoring cellular oxidative stress in liver injury. *Sci. Rep.* **2017**, *7*, 45374.
(53) Saito, C.; Zwingmann, C.; Jaeschke, H. Novel mechanisms of protection against acetaminophen hepatotoxicity in mice by glutathione and N-acetylcysteine. *Hepatology* **2010**, *51*, 246−254.
(54) Jaeschke, H.; Xie, Y.; McGill, M. R. Acetaminophen-induced liver injury: from animal models to humans. *J. Clin. Transl. Hepatol.* **2014**, *2*, 153−161.
(55) Wu, L.; Liu, J.; Li, P.; Tang, B.; James, T. D. Two-photon small-molecule fluorescence-based agents for sensing, imaging, and therapy within biological systems. *Chem. Soc. Rev.* **2021**, *50*, 702−734.
(56) Hinson, J. A.; Roberts, D. W.; James, L. P. Mechanisms of acetaminophen-induced liver necrosis. In *Adverse Drug Reactions*; Uetrecht, J., Ed.; Springer Berlin Heidelberg: Berlin, Heidelberg, 2010; pp 369−405.